New Astronomy 73 (2019) 101277

Contents lists available at ScienceDirect

New Astronomy

journal homepage: www.elsevier.com/locate/newast

Characteristic features in photoionization of Fe XIX

Sultana N. Nahar

Department of Astronomy, The Ohio State University, Columbus, OH 43210, USA

ARTICLE INFO

Keywords:
Atomic processes: Photoionization
Fe XIX
Stars: galaxies: line formation

ABSTRACT

Characteristic features of the resonances and background cross sections for photoionization (σ_{PI}) of oxygen-like iron ion, Fe XIX + h$\nu \rightarrow$ Fe XX + e, are demonstrated. The features are introduced by excitations of the core ion to states of n = 2,3,4 complexes in σ_{PI} of the ground, equivalent electron, and single valence electron excited states. Study from a large number of states is important to establish the general properties of photoionization for complex ions. This is the first detailed study of the ion with a complete set of σ_{PI} for 900 bound states with n $\leq$ 10 and $l \leq$ 9. The ion itself is of great interest for being detected in the x-ray to UV spectra of various astronomical objects. It is found that i) the ground and equivalent electron states have high peak narrow Rydberg resonances in the low energy region corresponding to n = 2 excitations only, ii) for other excited states the resonant features are stronger for core ion excitations to n = 3 complex compared to those for n = 2,4, iii) Seaton resonances due to photo-excitation of the core (PEC) are found most distinct in the energy region for dipole allowed excitation from n = 2 to n = 3 states, and iv) resonances with lower peaks in the energy region between n = 3 and n = 4 excitation indicate convergence. Computations were carried out in the R-matrix method using a large close coupling wavefunction expansion up to orbital 4f and 16 configurations. The present results should provide the data for precise modeling and applications.

1. Introduction

Photoionization is one most common process in the atmosphere, illuminated plasma, such as, in stars, galaxies and appear in absorption spectra. Photoionization of an ion, X^+, can be direct as

$$h\nu + X^+ \rightarrow e + X^{++}, \tag{1}$$

which gives the featureless background cross sections or through a two-step process,

$$e + X^{++} \leftrightarrow (X^+)^{**} \leftrightarrow \begin{cases} a)\ e{+}X^{++}(AI) \\ b)\ h\nu{+}X^+(DR) \end{cases} \tag{2}$$

shown indirectly through the collision process. When the photon energy matches to a state of the Rydberg series $(S_cL_c\pi_c)\nu l$ above the ionization energy, an intermediate doubly excited quasi-bound autoionizing state (as shown by double asterisks) is formed and breaks down either to autoionization (AI) where the interacting electron goes in to the continuum or to dielectronic recombination (DR) where it is captured by emission of a photon (e.g. Pradhan and Nahar, 2011). $(S_cL_c\pi_c)$ is an excited state of the core ion and νl is the outer electron quantum level and ν is the effective quantum number belonging to the excited core ion. An autoionizing state is manifested as a resonance in the process which can be calculated naturally by including the core excitation in the wave function such as considered in the close coupling (CC) approximation used in the present work. An isolated resonance can appear in the absorption spectra while overall cross sections impact the continuum and formation of lines.

Lines of Fe XIX are being detected from x-ray to far-UV spectra of various astronomical objects, such as, photoionized cool stars, x-ray binaries, and galaxies by the space observatories EXOSAT, ROSAT, Einstein, Ginga, ASCA, XMM-Newton, Chandra etc. Spectral analysis of the ion provides characteristics and phenomenal behaviors of the plasmas, such as, diagnostics of temperature and density for hot plasmas at 1–10 MK. Liedahl et al. (1990) found two diagnostic lines of Fe XIX in x-binaries and discussed (Liedahl et al., 1992) the importance of iron ions that prominently exist in high-temperature X-ray sources. Fe XIX is prominently seen in spectra of the Capella system (Brickhouse and Drake, 2000) and abundantly exists near the boundary of the radiative and convection zones (Bailey, 2015). Precise analysis of the line ratios of Fe XVII and Fe XIX in the observed spectra of the Capella system by Desai (2005) found to be at discrepant with the predicted values largely due to inaccurate atomic data of the radiative and collisional processes occurring in the plasmas. Their assessment of the Chandra x-ray spectra for the Capella system explained the

E-mail address: nahar.1@osu.edu, http://www.astronomy.ohio-state.edu/~nahar.
URL:

https://doi.org/10.1016/j.newast.2019.101277
Received 14 February 2019; Received in revised form 20 April 2019; Accepted 6 June 2019
Available online 07 June 2019
1384-1076/

importance of photoionization and electron-ion recombination processes of L-shell of iron ions. However the atomic data are scarce or inadequate and there is a special need for them for Fe XIX. Photoionization cross sections for the ion is also crucial for the solution of the solar plasma opacity as it is abundant in the boundary region of the radiative and convection zones where has been the focus of most studies (e.g. Bailey, 2015)

The earlier studies of photoionization of Fe XIX were carried out by Donnelly et al. (1999) and Zhang and Pradhan (2000) using Breit–Pauli R-matrix method. Both studies used a smaller close-coupling (CC) wavefunction expansion of 23 fine structure levels corresponding to 12 LS states and core ion excitations could go up to orbital 3s. The present work considers a much larger wavefunction expansion of 192 LS states where core ion can be excited up to 4f orbital, which can happen in high temperature plasmas where the ion exists. However, as explained later the number of states could be reduced on the physical ground based on the excitations that are forbidden transitions and hence contribute only to the background cross sections. Both Donnelly et al. (1999) and Zhang and Pradhan (2000) confined the study to the levels of the ground state of Fe XIX only. Donnelly et al. (1999) found some unusual resonant structures in two levels of the ground state present in the energy region of about 130–155 Ry, generated by the relativistic Breit-Pauli version of the R-matrix codes (Berrington et al., 1995) but not by the LS coupling version of the codes (Berrington et al., 1987). It is discussed in detail by Zhang and Pradhan (2000) who also used Breit–Pauli version but could not see those structures. Photoionization cross sections calculated by Donelly et al. also had much lower background cross sections than those obtained by Zhang and Pradhan.

Under the Opacity Project (The Opacity Project Team, 1995, 1996) the f-values were obtained by Butler and Zeippen (2019) for LS multiplets availabe at the Opacity Project database, TOPbase (TOPbase), and by Nahar (2011) for fine structure transitions but no photoionization cross sections were computed or available. This report presents an extensive calculation under the Iron Project for the photoionization cross sections of Fe XIX for a large number of bound states with a wavefunction expansion revealing features at high energies.

2. Theory

The close coupling (CC) approximation describes an atomic system as a system of (N+1) electrons where the core ion, also often called the target, of N-electrons is interacting with the (N+1)th electron. The total wave function, Ψ_E, of the (N+1) electrons system in a symmetry $SL\pi$ is represented by an expansion as

$$\Psi_E(e + ion) = A \sum_i \chi_i(ion)\theta_i + \sum_j c_j \Phi_j, \tag{3}$$

where in the first term the core ion eigenfunction, χ_i, is coupled with the (N+1)th electron function, θ_i. The sum is over the ground and excited states of the core ion. The (N+1)th electron with kinetic energy k_i^2 is in a channel labeled as $S_iL_i\pi_i k_i^2 \ell_i(SL\pi)$. In the second sum, the Φ_js are bound channel functions of the (N+1)-electrons system that account for short range correlation and the orthogonality between the continuum and the bound electron orbitals.

The Hamiltonian of (N+1)-electrons system in Rydberg unit (1/2 of Hartree) is written as

$$H_{N+1} = \sum_{i=1}^{N+1} \left\{ -\nabla_i^2 - \frac{2Z}{r_i} + \sum_{j>i}^{N+1} \frac{2}{r_{ij}} \right\} + H_{N+1}^{\rm mass} + H_{N+1}^{\rm Dar} \tag{4}$$

Although the computations were carried out in LS coupling, two one-body relativistic correction terms, the mass correction, $H^{\rm mass} = -\frac{\alpha^2}{4}\sum_i p_i^4$ and Darwin, $H^{\rm Dar} = \frac{Z\alpha^2}{4}\sum_i \nabla^2(\frac{1}{r_i})$, were included for improvement.

Substitution of the CC wavefunction $\Psi_E(e + ion)$ in the Schrodinger equation

$$H_{N+1}\Psi_E = E\Psi_E \tag{5}$$

introduces a set of coupled equations that are solved using the R-matrix method. The details of the R-matrix method in the CC approximation can be found, e.g., in Burke and Robb (1975), Seaton (1987), Berrington et al. (1987), and summarized in Pradhan and Nahar (2011). The solution of the equations is a continuum wave function, Ψ_F, for an electron with positive energies (E > 0), or a bound state, Ψ_B, at a negative total energy (E ≤ 0).

Transition matrix elements for photoionization, $< \Psi_B||\mathbf{D}||\Psi_F >$ where $\mathbf{D} = \sum_i \mathbf{r}_i$ is the dipole operator and the sum is over the number of electrons, are obtained from the bound Ψ_B and continuum Ψ_F wave functions. The transition matrix element gives the generalized line strength **S** as

$$\mathbf{S} = |<\Psi_j\|\mathbf{D}_L\|\Psi_i>|^2 = \left| \left\langle \psi_f | \sum_{j=1}^{N+1} r_j | \psi_i \right\rangle \right|^2, \tag{6}$$

where Ψ_i and Ψ_f are the initial and final state wave functions and photoionization cross section (σ_{PI}) is obtained as,

$$\sigma_{PI} = \frac{4\pi^2}{3c}\frac{1}{g_i}\omega\mathbf{S}, \tag{7}$$

where g_i is the statistical weight factor of the bound state and ω is the incident photon energy. The complex resonant structures in photoionization result from channel couplings between continuum channels that are open ($k_i^2 > 0$), and ones that are closed ($k_i^2 < 0$), at electron energies k_i^2 corresponding to autoionizing states of the Rydberg series, $S_iL_iJ_i\pi_i\nu\ell$ converging to the thresholds of the target, that is, core ion.

3. Computation

The computation of the photoionization cross sections was carried out using the R-matrix package of codes (Berrington et al., 1987; 1995) in the LS coupling mode. The original codes (Burke and Taylor, 1975) were extended extensively under the Opacity (1995, 1996) and the Iron Projects (Hummer et al., 1993). The R-matrix method involves number of stages of computations. It starts with stage 1, named STG1 which takes the wave function of the core or the residual ion obtained from an atomic structure calculation as the input. In the present work these wavefunctions for core ion Fe XX were obtained using the atomic structure code SUPERSTRUCTURE (SS) (Eissner et al., 1974; Nahar et al., 2003). SS uses Thomas–Fermi–Dirac–Amadi approximation with inclusion of relativistic effects in Breit–Pauli approximation.

3.1. Consideration core ion states

A set of 16 configurations of Fe XX: 1) $2s^22p^3$, 2) $2s2p^4$, 3) $2p^5$, 4) $2s^22p^23s$, 5) $2s^22p^23p$, 6) $2s^22p^23d$, 7) $2s^22p^24s$, 8) $2s^22p^24p$, 9) $2s^22p^24d$, 10) $2s^22p^24f$, 11) $2s2p^33s$, 12) $2s2p^33p$, 13) $2s2p^33d$, 14) $2s2p^34s$, 15) $2s2p^34p$, 16) $2s2p^34d$ with filled $1s$ orbital in all configurations and Thomas-Fermi scaling parameters for the orbitals: 1.35(1s), 1.25(2s), 1.12(2p), 1.07(3s), 1.05(3p), 1.0(3d), 1.0(4s), 1.0(4p), 1.0(4d), 1.0(4f) were used to obtain the optimized wavefunctions of the ion. All configurations were treated spectroscopic and resulted in 192 LS states with 445 fine structure levels. The first 8 states of Fe XX belonging to $n = 2$ complex are bound with energies up to 18 Ry relative to the ground state. The next set of states of $n = 3$ complex start after a large energy gap of 66.5 Ry, about 48 Ry above of those of $n = 2$ complex. There is another energy gap of over 7 Ry between states of $n = 3$ and $n = 4$ complexes.

Being a highly ionized iron ion, existence of Fe XIX is expected to be in the high temperature plasmas and hence inclusion of highly excited core ion states up to $n = 4$ is important to ensure the contribution of the high energy features of the ion. The choice also enables verification of

the resonance convergence features with higher n (Nahar and Pradhan, 2016; Nahar, 2018).

A suitable set of target states, instead of all 192 states of Fe XX but covering the corresponding energy range, was chosen for the large scale computation. The set includes the first 17 states, which is all 8 states of $n = 2$ and 9 from $n = 3$ complexes, in energy order and then consideration for selection of states was made based on the physical properties that affect the features.

The Rydberg series of resonances belonging to core ion excitations that are dipole allowed from the ground state are more prominent than others. Resonances of states that do not couple to the ground state of the core ion are usually suppressed. A dipole allowed excitation in the core ion has an additional effect which is the formation of a Seaton resonance (Yu and Seaton, 1987; Pradhan and Nahar, 2011). Since the ground state of Fe XX is a S state, $^4S^o$, there is only one state which is ^4P, instead of three different L states, available for the dipole allowed transitions. This reduced the set significantly. There are 13 excited ^4P states in the present set. The selected set of target states includes all 13 of them and their adjacent states.

The next criteria of selection is that an odd parity state which will not couple to the ground state $^4S^o$ to form any resonance and does not have noticeable energy gap with the adjacent states for any impact on the background can be eliminated. With these considerations, 58 states were selected as listed in Table 1. The calculated energies of the states are also compared with the observed energies (Sugar and Corliss, 1985) available at the compiled table of the NIST (nist: http://www.nist.gov/pml/data/asd.cfm). The observed energies of the fine structure levels were statistically averaged to obtain the LS term energies before comparison. For more accurate positions of the resonances, calculated energies were replaced by the available observed energies in the Hamiltonian. The agreement between the observed and calculated energies is within a few percent for most energies.

The first term of the wavefunction Eq. (3) included the 58 states coupled with partial waves of angular momenta of $0 \le l \le 9$ of the interacting electron. The second term of Ψ included 104 configurations of Fe XIX with minimum and maximum electron occupancies were as specified within the parenthesis of the orbitals: 1s (2-2), 2s (0-2), 2p (2-6), 3s (0-2), 3p (0-2), 3d (0-2), 4s (0-1), 4p (0-1), 4d (0-1), 4f (0–1). Computations are carried out for all states with angular momenta, $0 \le L \le 9$ for septets, $0 \le L \le 11$ for quintets, triplets and singlets of Fe XIX. However, no bound states of the septets were found. The resonances in the photoionization in the low energy region at and near the ionization threshold were delineated at a very fine energy mesh. Over 40,000 energy points were considered for the photoionization of each state. They were obtained by the running the computational jobs in smaller energy bins.

4. Results and discussions

Characteristic features of photoionization of Fe XIX (Fe XIX + $h\nu \rightarrow$ Fe XX + e) are presented from a study of a large number of bound states of the ion. These features establish properties of the photoionization process of complex ions. Very limited amount of data with details of the process for Fe XIX are available. The available σ_{PI}, by Donnelly et al. (1999) and Zhang and Pradhan (2000), are focused to the levels of the ground state and for the low lying resonances only. Compared to the earlier work, the present results i) consider a much larger wavefunction expansion extending to high energy region needed for the study of high temperature plasmas where the ion is more abundant, ii) illustrate various features in wide range of energies that belong to ground, equivalent electron and single valence electron excited states of the ion, iii) study convergence of resonances with higher core ion excitations, iv) comprise a data set of photoionization cross sections of 900 bound states that is complete for all practical application for various astrophysical and laboratory plasmas.

The present work has found 900 bound states of Fe XIX with $n \le 10$ and $l \le 9$ for which photoionization cross sections have been obtained. All calculated energies have been identified spectroscopically through analysis of quantum defects and dominant contributing channels using a program ELEVID (Nahar, 1993). The energies are checked with the observed energies (Sugar and Corliss, 1985) compiled by the NIST (2015) table (nist). The observed fine structure energies at the NIST website were statistically averaged for the comparison as given in Table 2. As seen, the calculated energies agree with the observed values within a few percent for all cases except two cases where they are higher than 5%. The largest percent difference, 11.43, is with state $2s^22p^3(^2P^o)6d(^3D^o)$. The differences often come from the way states are identified. While the physics is correct based on the number of configurations used for optimization of the state, the percentage contribution of the configurations depends also on the method. It could be such a case for the state. The other calculated LS bound energies, 633 in total, from R-matrix method obtained by Butler and Zeippen (2019) are available at the Opacity Project database, TOPbase (TOPbase). They are in general in good agreement with the present energies but have somewhat higher percent differences with the observed energies. For example, the energies of the ground configuration is 1.06592 Ry ^3P, 105.665 Ry for ^1D, 104.587 Ry for ^1S states.

Characteristic features in σ_{PI} are illustrated below.

4.1. Photoionization of ground and equivalent electrons states

Photoionization features of the three states of the ground configuration of Fe XIX, $2s^22p^4(^3P, ^1D, ^1S)$, are shown in Fig. 1 (a–c). They show that visible resonances exist in the low energy region within $n = 2$ complex of the core ion (complex limit is pointed by an arrow). There is very little impact on the photoionization cross sections (σ_{PI}) from core ion excitations to states of $n = 3$ and 4 complexes which, as mentioned in the computation section, lie significantly high. These features agree with those in LS coupling cross sections of Donnelly et al. (1999) and Breit–Pauli R-matrix (BPRM) cross sections by Zhang and Pradhan (2000). The present background cross sections agree with those of Zhang and Pradhan (2000) while those by Donnelly et al. (1999) are much lower. Both group used a wavefunction expansion that includes states of $n = 2$ complex and 3s states of $n = 3$ complex of the core ion. They do not see the small bump around 160 Ry of the present work. The reason could be inclusion of orbitals 3s,3p,3d states in the present work. Both the earlier papers discuss in detail the comparison of the cross sections of the ground state obtained by them and others and hence are not repeated here.

The resonances at and near the threshold region of the photoionization cross section (σ_{PI}) of the three states correspond to the autoionizing Rydberg series of states, $^2D^o\nu l$ and $^2P^o\nu l$, belonging to the first two excitations $^2D^o$ and $^2P^o$ of the core ion (the first two arrows in the figure). At the core ion excitation threshold of ^4P (the 3rd arrow) which is a dipole allowed state to the ground state $^4S^o$ there is a resonance for all states and a slight enhancement for ^3P state. Slight enhancement is also noticed at the ^2S threshold (the 4th arrow).

Although few in number, the equivalent electron states of an ion often contribute significantly in low and high temperature plasmas because of their prominent low energy resonances in the low energy near ionization thresholds and relatively higher background cross section. All three states of Fig. 1 are equivalent states. Fig. 2 presents features in σ_{PI} of three equivalent electron states of two excited configurations, a) $2s2p^5(^3P^o)$, b) $2s2p^5(^1P^o)$, and c) $2p^6(^1S)$.

Similar to Fig. 1, the three equivalent electron states of Fig. 2 show appearance of Rydberg series of resonances belonging to the excited states of $n = 2$ complex of the core ion. One exception here is the extension of prominent resonances up to limit of the $n = 2$ states of the core ion compared to those for the ground configuration where they do not. Core ion excitations to $n = 3,4$ states have insignificant contribution to σ_{PI}.

Table 1
Energies (E_t) of core ion Fe XX states included in the wave function expansion of Fe XIX. Calculated energies are compared with those from the NIST tabulations (http://physics.nist.gov/PhysRefData/ASD/levels_form.html).

	State		E_t(Ry)	E_t(Ry)	%diff		State		E_t(Ry)	E_t(Ry)	%diff
			SS	NIST					SS	NIST	
1	$2s^22p^3$	$^4S^o$	0.0	0.0	0.	46	$2s2p^33p$	^2D	77.0639		
2	$2s^22p^3$	$^2D^o$	1.5091	1.4683	2.79	47	$2s2p^33d$	$^4D^o$	78.7272		
3	$2s^22p^3$	$^2P^o$	2.7698	2.7549	0.54	48	$2s2p^34d$	$^4D^o$	98.9943		
4	$2s2p^4$	^4P	7.2235	7.2029	0.30	49	$2s^22p^24s$	^4P	89.1190		
5	$2s2p^4$	^2D	9.6995	9.5869	1.17	50	$2s^22p^24s$	^2P	89.2434		
6	$2s2p^4$	^2S	10.9879	10.8920	0.01	51	$2s^22p^24d$	^4P	91.7275	90.621	1.21
7	$2s2p^4$	^2P	11.7840	11.6184	1.42	52	$2s^22p^24f$	$^4D^o$	91.2580		
8	$2p^5$	$^2P^o$	18.3096	18.1380	0.95	53	$2s2p^34s$	$^4S^o$	91.8962		
9	$2s^22p^23s$	^4P	66.4611	66.2742	0.28	54	$2s2p^34p$	^4P	92.6497		
10	$2s^22p^23s$	^2P	66.6114			55	$2s2p^34p$	^4P	95.4711		
11	$2s^22p^23s$	^2D	67.9889	67.7072	0.42	56	$2s2p^34p$	^4P	96.3309		
12	$2s^22p^23p$	$^2S^o$	67.7034			57	$2s2p^34p$	^4P	98.1733		
13	$2s^22p^23p$	$^4D^o$	67.9864			58	$2s2p^34d$	$2G^o$	98.9904		
14	$2s^22p^23p$	$^4P^o$	68.1569								
15	$2s^22p^23p$	$^2D^o$	68.3764								
16	$2s^22p^23p$	$^4S^o$	68.4161								
17	$2s^22p^23p$	$^2P^o$	68.6719								
18	$2s2p^33s$	$^6S^o$	68.7384								
19	$2s^22p^23s$	^2S	69.4051	68.8371	0.83						
20	$2s^22p^23p$	$^23^o$	69.1895								
21	$2s^22p^23p$	$^2D^o$	69.6526								
22	$2s^22p^23p$	$^2P^o$	69.9494								
23	$2s2p^33s$	$^4S^o$	69.9944								
24	$2s^22p^23d$	^4F	70.7735	69.9124	1.24						
25	$2s^22p^23d$	^2P	70.4365								
26	$2s^22p^23d$	^4D	71.0644	70.6414	0.60						
27	$2s2p^33p$	^6P	70.6388								
28	$2s^22p^23d$	^4P	71.5391	71.0971	0.62						
29	$2s2p^33p$	^4P	71.3530								
30	$2s2p^33s$	$^4D^o$	71.7815								
31	$2s^22p^23d$	^2F	72.6902	71.8947	1.11						
32	$2s^22p^23d$	^2P	72.0264	72.6007	0.79						
33	$2s^22p^23d$	^2S	72.1583	72.8558	0.96						
34	$2s2p^33d$	$^6D^o$	72.7361								
35	$2s^22p^23d$	^2D	72.0383	71.5290	0.77						
36	$2s2p^33p$	^4D	73.4942								
37	$2s2p^33d$	$^4D^o$	73.7854								
38	$2s2p^33p$	^4P	74.3545								
39	$2s2p^33s$	$^2D^o$	74.8718								
40	$2s2p^33p$	^4P	74.9873								
41	$2s2p^33d$	$^4F^o$	75.5614								
42	$2s2p^33d$	$^4G^o$	75.7194								
43	$2s2p^33s$	$^2P^o$	75.8075								
44	$2s2p^33p$	^2P	76.4825								
45	$2s2p^33p$	^4P	76.6062								

4.2. Impact of n = 2,3,4 excitations on photoionization

Figs. 1 and 2 show insignificant contribution on the photoionization by the higher excitations of the core ion. This is often the case with the ground and equivalent electron states (Nahar, 2018; 2019). However, the impact is much more prominent in photoionization of excited states with a single valence electron. It has been established for various cases that resonances belonging to the core excitations to $\Delta n = 1$ are much stronger than $\Delta n = 0,2$ (Nahar, 2018). This is illustrated for two excited states of Fe XIX, $2s2p^4 3d(^5P)$ and $2p^5 3s(^3P^o)$, in Fig. 3.

The impact of the excitations is better illustrated in the log scale than in the linear scale as shown in the Fig. 3 where the top two panels (a-i) and (a-ii) present photoionization cross section of the excited state $2s2p^4\,{}^4P3d(^5P)$, panel i) in logarithmic and panel ii) in linear scale, and the panels (b-i) and (b-ii) are for the excited $2p^5 3s(^3P^o)$ state. There are few common features demonstrated in the figure. i) The region of ionization threshold to low energy resonances appear with almost zero background but the background is enhanced either by a dipole allowed transition in the core ion for ^5P state (blue arrows) or at the highest excitation threshold of the $n = 2$ complex for $^3P^o$ state. These features are common but do not always exist. ii) Dominance of strong high peak Rydberg resonances in the energy region between $n = 2$ and $n = 3$ (arrows in red) excitation limits of the core ion. The peaks are reaching higher than those for $n = 2$ and $n = 4$ complexes by order of magnitudes implying higher contributions in photoabsorption from this region in various applications. ii) Enhancement in the background due to core ion excitations to states in $n = 2,3,4$ complexes are more distinct at the energies for dipole allowed transitions, that is, $4S^o - {}^4P$ (blue arrows). iii) The enhancement with higher excited core ion states does not necessarily continue for all states. As seen in panels (a-i) and (b-i) that while enhancement continues to some extent for the $2s2p^4\,{}^4P3d(^5P)$ state it decreases for the $2p^5 3s(^3P^o)$ state. iv) The enhancement feature of the background is more distinct in log scale compared to that in linear scale as seen for the two states in panels of Fig. 3. So if the magnitude of the background cross section remains low as seen in panels a-ii) and b-ii), the individual impact may not be significant, but total contribution can be significant when all states are combined. v) Convergence characteristic of strength of resonances can be noted in the energy region between $n = 3$ and 4 complexes where the resonances have become much weaker.

Table 2
Comparison of calculated R-matrix (RM) energies (E_c) Fe XIX states with those from the NIST tabulations (http://physics.nist.gov/PhysRefData/ASD/levels_form.html). An asterisk next to the measured energy indicate incompleteness of the set of the observed fine structure levels.

Configuration	State	E_c(Ry) NIST	E(Ry) RM	%Diff
$2s^22p^4$	^3P	107.552124	107.03939	0.48
$2s^22p^4$	^1D	106.361305	106.08289	0.26
$2s^22p^4$	^1S	104.937111	104.95631	0.02
$2s2p^5$	$^3P^o$	99.193665	98.72209	0.43
$2s2p^5$	$^1P^o$	96.348778	95.91055	0.45
$2p^6$	^1S	88.451920	87.88260	0.64
$2s^22p^3(^4S^o)3s$	$^3S^o$	47.027351	46.36215	1.41
$2s^22p^3(^2D^o)3s$	$^3D^o$	45.918644	45.28954	1.37
$2s^22p3(^2D^o)3s$	$^1D^o$	45.624001	45.28954	0.73
$2s^22p^3(^2P^o)3s$	$^3P^o$	44.591232	44.51707	0.17
$2s^22p^3(^2P^o)3s$	$^1P^o$	44.247986	44.25940	0.03
$2s^22p^3(^4S^o3/2)3d$	$^3D^o*$	41.842243	41.25042	1.41
$2s^22p^3(^2D^o3/2)3d$	$^3P^o*$	40.739609	39.79494	2.32
$2s^22p^3(^2D^o5/2)3d$	$^3D^o*$	40.468506	39.93793	1.31
$2s22p^3(^2D^o5/2)3d$	$^1F^o$	40.019707	40.44976	1.07
$2s^22p^3(^2P^o1/2)3d$	$^3F^o*$	39.942249	40.44976	1.27
$2s^22p^3(^2P^o3/2)3d$	$^3D^o$	38.992405	39.13977	0.38
$2s^22p^3(^2P^o3/2)3d$	$^1P^o$	38.589016	38.27849	0.80
$2s^22p^3(^4S^o3/2)4d$	$^3D^o$	23.651525	23.14953	2.12
$2s^22p^3(^2D^o3/2)4d$	$^3F^o*$	22.614504	21.79369	3.63
$2s^22p^3(^2D^o3/2)4d$	$^3D^o*$	22.384867	21.67439	3.17
$2s^22p^3(^2D^o5/2)4d$	$^1F^o$	22.085968	21.79369	1.32
$2s^22p^3(^2D^o5/2)4d$	$^1D^o$	22.085968	21.67439	1.86
$2s^22p^3(^2P^o1/2)4d$	$^3F^o*$	21.450359	21.03631	1.93
$2s^22p^3(^2P^o1/2)4d$	$^3D^o*$	21.384293	20.91988	2.17
$2s^22p^3(^2P^o3/2)4d$	$^1F^o$	20.855759	21.03631	0.97
$2s^22p^3(^2P^o3/2)4d$	$^3P^o*$	20.819307	21.00578	0.90
$2s^22p^3(^2P^o3/2)4d$	$^1P^o$	20.664392	21.65069	4.77
$2s^22p^3(^4S^o)5d$	$^3D^o*$	15.041873	14.62611	2.76
$2s^22p^3(^2D^o)5d$	$^3D^o*$	13.766099	13.25358	3.72
$2s^22p^3(^2D^o)5d$	$^1D^o$	13.492719	13.25358	1.77
$2s^22p^3(^2D^o)5d$	$^1F^o$	13.219338	13.30053	0.61
$2s^22p^3(^2D^o)5d$	$^3F^o*$	12.945958	13.30053	2.74
$2s^22p^3(^2P^o)5d$	$^3D^o*$	12.353635	11.94638	3.30
$2s^22p^3(^2P^o)5d$	$^3F^o*$	12.216945	12.00431	1.74
$2s^22p^3(^2P^o)5d$	$^3P^o*$	12.216945	12.81029	4.86
$2s^22p^3(^2P^o)5d$	$^1F^o$	12.216945	12.00431	1.74
$2s^22p^3(^2P^o)5d$	$^1P^o$	12.125818	12.93412	6.67
$2s^22p^3(^4S^o)6d$	$^5D^o*$	10.576664	10.21982	3.37
$2s^22p^3(^4S^o)6d$	$^3D^o*$	10.303284	10.13267	1.66
$2s^22p^3(^2P^o)6d$	$^3D^o*$	9.847651	8.72231	11.43
$2s^22p^3(^2D^o)6d$	$^1F^o$	7.387228	7.45554	0.92

4.3. Seaton resonances in photoionization of excited states

One common feature in photoionization of excited states with a single valence electron is the presence of Seaton resonances due to photoexcitation-of-core (PEC) to dipole allowed states (Yu and Seaton, 1987). A Seaton resonance is introduced when the core absorbs the photon before leading to ionization and hence the energy positions for these resonances remain the same for all excited states. They are typically more distinct in highly excited states. These resonances can be wide with enhanced background embedded in narrow Rydberg resonances.

Fig. 4 presents σ_{PI} of three highly excited levels illustrating features of Seaton resonances. The levels are arranged in low to high energy order of their ionization potential, (a) $2s^22p^3(^4S^o)10f(^5F)$, (b) $2s^22p^3(^2P^o)5f(^3D)$, and (c) $2s^22p^3(^2D^o)4d(^3S^o)$. The arrows point the 13 energy positions that can form Seaton resonances by PEC to dipole allowed transitions $^4S^o - ^4P$ of the ground state (see Table 1 for the 13 ^4P states). The first Seaton resonance appears in the top panel of Fig. 4(a) only since the ionization threshold of this highly excited ^5F state is below this PEC threshold. All three states in the figure show widening enhancement around the PEC positions in the background cross sections. The combined contributions of them will make σ_{PI} at higher energy important in various applications.

It may be noted that the second background enhancement in the middle panel for ^3D state peaks around 85 Ry, not exactly at the PEC position of about 89 Ry. The reason is not clear except that the shift could be from interference of Rydberg resonances along with the Seaton resonance. This effect is noticed for a number of excited states. The other point of significance is the rise in the background to $n = 4$ excitations, lowest for the highest excited state ^5F (Fig. 4a) and highest for

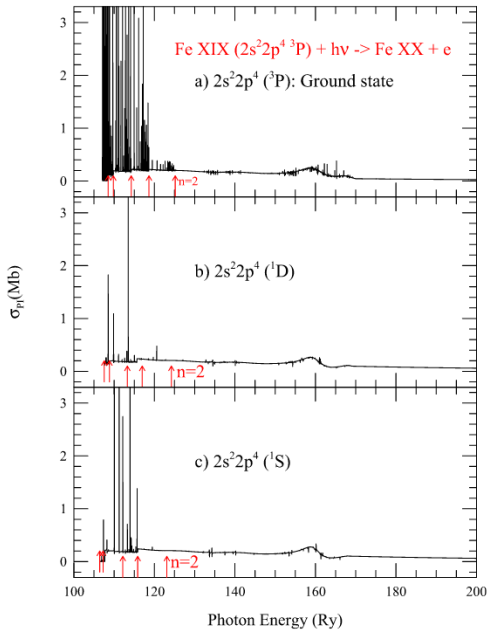

Fig. 1. Photoionization cross sections σ_{PI} of a) the ground state $1s^2\,2s^2\,2p^4(^3P)$ and the lowest excited states b) $1s^2\,2s^2\,2p^4(^1D)$ and c) $1s^2\,2s^2\,2p^4(^1S)$ of the ground configuration of Fe XIX. The prominent resonances belong to the excitations of the core ion in $n = 2$ complex.

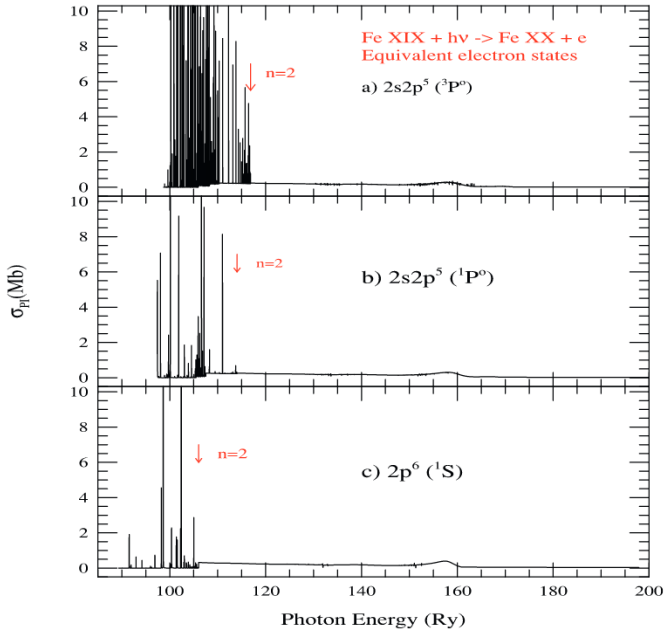

Fig. 2. Photoionization cross sections σ_{PI} of the three equivalent electron states of Fe XIX: a) $1s^2\,2s\,2p^5(^3P^o)$, b) $1s^2\,2s\,2p^5(^1P^o)$, and c) $1s^2\,2p^6(^1S)$, of Fe XIX. The "$n = 2$" arrows point the threshold limit to all resonances belonging to states: $2s^22p^3(^2D^o, ^2P^o)$, $2s2p^4(^4P, ^2D, ^2S, ^2P)$, $2p^5(^2P^o)$ of $n = 2$ complex of the core ion Fe XX. The plots show no impact on consideration of the higher excited states of the core ion.

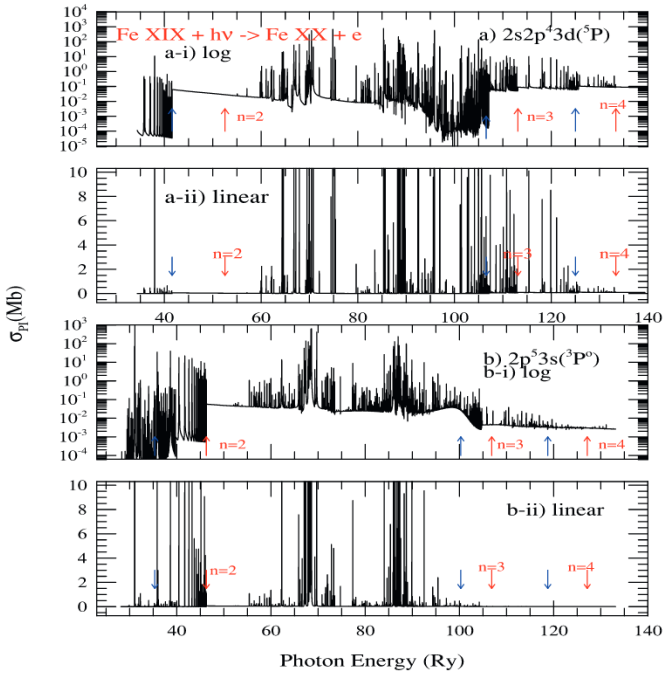

Fig. 3. Demonstration of the impact of the core ion excitations to states in n = 2,3,4 complexes on photoionization cross sections σ_{PI} of two excited states of Fe XIX: a) $2s2p^4 3d(^5P)$ and b) $2p^5 3s(^3P^o)$. Cross section of each state is plotted twice, in i) log and ii) linear scales to illustrate the resonant structures and enhancement of the background at core excited thresholds (arrows in the panel).

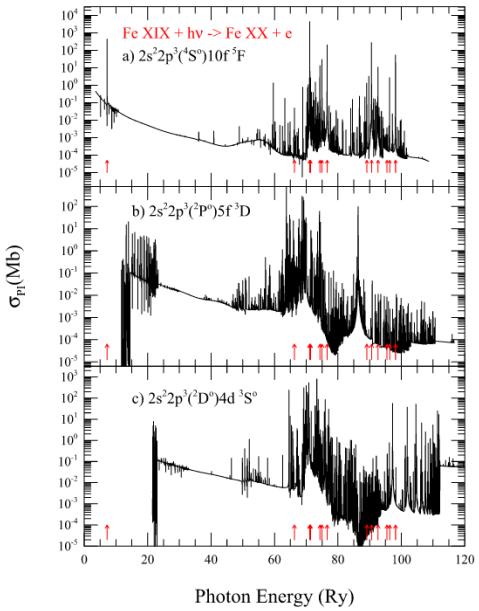

Fig. 4. Photoionization cross sections σ_{PI} of three highly excited states a) $2s^2 2p^3(^4S^o)10f(^5F)$, b) $2s^2 2p^3(^2P^o)5f(^3D)$, c) $2s^2 2p^3(^2D^o)4d(^3S^o)$, of Fe XIX illustrating prominent Seaton resonances introduced by photoexcitation of the core (PEC) from the ground to various electric dipole allowed states. The energy positions of these resonances are pointed out by arrows. These resonances interfere with Rydberg series of resonances and enhance the background cross section.

the lowest excited state $^3S^o$. The trend is that with much higher excited states, the background shows less variations.

5. Conclusion

Characteristic features in photoionization cross sections of Fe XIX are presented in detail from a study of 900 bound states. The features are classified for the ground state, equivalent states with excited configurations, impact of higher excitation of the core ion on the resonances and background cross sections of photoionization of excited states, Seaton resonances, and convergence of resonant features with higher core excitations. These σ_{PI} have been obtained from a wavefunction expansion that includes core ion excitations of n = 2,3,4 complexes. The photoabsorption features at high energies due to higher core excitations are important for precise modeling if the ion exists in high temperature plasmas. It is found that resonant features due to Δn = 1 (n = 3) excitations dominate the most and become weaker with Δn = 2 (n = 4). All bound states were identified spectroscopically and most show good agreement in less than 5% with experimental energies. The overall agreement indicates higher accuracy of the wavefunctions. Comparison with various experiments carried out at different set-ups for various ions show that R-matrix photoionization cross sections can be very accurate in terms of resonant positions and peaks, backgrounds (e.g. Nahar, 2004, Simon, 2010, Nahar et al., 2017). The present cross sections are from LS coupling without the fine structure and hence characteristics are statistical averaged. Although the resonances have been resolved with large number of energy points, there can be some narrow resonances missing that are not allowed in LS coupling but allowed in fine structure. There is no exact way to find the accuracy of the cross sections of all states, but based on the above explanations and consideration of large number configurations for Fe XIX, the data should be accurate within 15–20% for all practical applications. This is the first detailed study of photoionization of Fe XIX for a large number of states with n $\leq$ 10.

All photoionization data are available electronically from NORAD-Atomic-Data (NaharOSURadiativeAtomicData) website: www.norad.astronomy.ohio-state.edu/.

Acknowledgments

This work was supported partially by the grants of NSF AST-1312441 and DOEDE-SC0012331. The computational work was carried out at the Ohio Supercomputer Center in Columbus Ohio.

References

Bailey, J.E., et al., 2015. Letter 517, 56–59. (22 authors) Nature
Berrington, K.A., Burke, P.G., Butler, K., Seaton, M.J., Storey, P.J., Taylor, K.T., Yu, Y., 1987. Comput. Methods. J. Phys. B 20, 6379–6397.
Berrington, K.A., Eissner, W., Norrington, P.H., 1995. Comput. Phys. Commun. 92, 290–420.
Brickhouse, N.S., Drake, J., 2000. Rev. Mex. AA Ser. Conf. 9, 24.
Burke, P.G., Robb, W.D., 1975. Adv. At. Mol. Phys. 11, 143–214.
Burke, P.G., Taylor, K.T., 1975. J. Phys. B 8, 2620.
Butler, K., Zeippen, C. J.. Unpublished, Data available at the OP database TOPbase.
Desai, P., et al., 2005. ApJ 625, L59.
Donnelly, D., Bell, K.L., Keenan, F.P., 1999. MNRAS 307, 595.
Eissner, W., Jones, M., Nussbaumer, N., 1974. Comput. Phys. Commun. 8, 270.
Hummer, D.G., Berrington, K.A., Eissner, W., K., P.A., Saraph, H.E., Tully, J.A., 1993. Astron. Astrophys. 279, 298–309.
Liedahl, D.A., Kahn, S.M., Osterheld, A.L., Goldstein, W.H., 1990. ApJ 350, L37.
Liedahl, D.A., Kahn, S.M., Osterheld, A.L., Goldstein, W.H., 1992. ApJ 391, 306.
Nahar, S.N., 1993. Phys. Scr. 48, 297.
Nahar, S.N., 2004. Phys. Rev. A 69, 042714.
Nahar, S.N., 2011. At. Data Nucl. Data Tables 97, 403–425.
Nahar, S.N., 2018. Astron. Soc. Pac. Conf. Ser. 515, 93–103. (Editors: C. Mendoza, S. Turck-Chieze, J. Colgan, 2018)
Nahar, S.N., 2019. New Ast. 67, 97–102.
Nahar, S.N., Eissner, W., Chen, G.X., Pradhan, A.K., 2003. Astro. Astrophys. 487, 789.
Nahar, S.N., Hernández, E.M., Hernández, L., Antillón, A., Morales-Mori, A., González, O., Covington, A.M., Chartkunchand, K.C., Hanstorp, D., Juárez, A.M., Hinojosa, G.,

2017. JQSRT 187, 215–223.
Nahar, S.N., Pradhan, A.K., 2016. Phys. Rev. Lett. 116, 235003.
NIST (National Institute of Standards and Technology), 2015. NIST Atomic Spectra Database (ver.5.3). MD website, Gaithersburg. http://physics.nist.gov/PhysRefData/ASD/levels_form.html
Pradhan, A.K., Nahar, S.N., 2011. Atomic Astrophysics and Spectroscopy (AAS). Cambridge University Press.
Seaton, M.J., 1987. J. Phys. B 20, 6363–6378.
Simon, M.C., et al., 2010. J. Phys. B 43, 065003.
Sugar, J., Corliss, C., 1985. J. Phys. Chem. 1664. Ref. Data 14, Suppl. 2
The Opacity Project Team, 1995. The Opacity Project. Institute of Physics Publishing. Vol 1. Vol. 2, (1996)
Yu, Y., Seaton, M.J., 1987. J. Phys. B 20, 6409.
Zhang, H.L., Pradhan, A.K., 2000. Mon. Not. R. Astron. Soc. 313, 13.